WAVELET-BASED IMAGE CODING USING ALLPASS FILTERS

Xi Zhang†, Seiya Kamimura and Toshinori Yoshikawa

Department of Electrical Engineering
Nagaoka University of Technology
Nagaoka, Niigata 940-2188 Japan
† E-mail: xiz@nagaokaut.ac.jp

ABSTRACT

In this paper, an effective implementation of allpass-based wavelet filters is presented for image compression. Since the wavelet bases used here are both orthonormal and symmetric, it can be expected to get a better compression performance than biorthogonal wavelet bases. Furthermore, the proposed allpass-based wavelet filters are IIR filters, thus it is known that the computational complexity in implementation is lower than FIR filters. Finally, it is shown through experimental results that the proposed allpass-based wavelet filters have a lower computational complexity than the conventional compact-supported wavelet filters, such as the popular Daubechies's 9/7-tap wavelet, with a comparable compression performance.

Keywords: Image Coding, Orthonormal Symmetric Wavelet Basis, Allpass Filter, IIR Filter.

1. INTRODUCTION

In the past decade, wavelet-based image coding has been extensively studied and applied in JPEG2000 and MPEG4. In the wavelet-based image coding scheme, two-band PR (perfect reconstruction) filter banks play a very important role [6]. To avoid redundancy between subimages, the PR filter banks should be orthonormal. Additionally, the analysis and synthesis filters are required to have an exactly linear phase (corresponding to symmetric wavelet bases), since linear phase filters allow us to use simple symmetric extension methods to accurately handle the boundaries of finite-length signals [5]. Unfortunately, there are no nontrivial orthonormal linear phase PR filter banks with FIR (finite impulse response) filters, except for the Haar basis [6]. To achieve a good compression performance, a reasonable regularity is necessary for wavelet bases. Therefore, at least one of the above-mentioned conditions has to be given up to get more regularity than the Haar basis. For example, the popular Daubechies's 9/7-tap wavelet basis is biorthogonal and the orthonormality requirement is relaxed [6]. On the other hand, it is known in [8] that IIR (infinite impulse response) wavelet filters can simultaneously satisfy both the orthonormality and linear phase requirements. A class of IIR orthonormal symmetric wavelet filters has been proposed in [8] by using allpass filters, and a closed-form solution for the maximally flat wavelet filters is given in [11] and [12].

In this paper, we present an effective implementation of the allpass-based wavelet filters for image compression. Since such allpass-based wavelet filters are both orthonormal and exactly linear phase, it can be expected to obtain a better compression performance than the conventional biorthogonal wavelet filters. Furthermore, IIR filters have a lower computational complexity in implementation and more degrees of freedom in design than FIR filters, in general. Finally, it is shown through experimental results that the allpass-based wavelet filters proposed in this paper have a lower computational complexity than the conventional compact-supported wavelet filters, such as the popular Daubechies's 9/7-tap wavelet, with a comparable compression performance.

2. ORTHONORMAL SYMMETRIC WAVELET FILTERS

It is well-known [1]∼[4] that wavelet bases can be generated by two-band PR filter banks $\{H(z), G(z)\}$, where $H(z)$ is a lowpass filter and $G(z)$ is highpass. The orthonormality condition that $H(z)$ and $G(z)$ must satisfy is

$$\begin{cases} H(z)H(z^{-1}) + H(-z)H(-z^{-1}) = 1 \\ G(z)G(z^{-1}) + G(-z)G(-z^{-1}) = 1 \\ H(z)G(z^{-1}) + H(-z)G(-z^{-1}) = 0 \end{cases} . \quad (1)$$

When symmetric wavelet bases are needed, $H(z)$ and $G(z)$ must have an exactly linear phase. In [8], Herley

and Vetterli have proposed a class of orthonormal symmetric wavelet filters by using real allpass filters, i.e.,

$$\begin{cases} H(z) = \frac{1}{2}\{A(z^2) + z^{-2K-1}A(z^{-2})\} \\ G(z) = \frac{1}{2}\{A(z^2) - z^{-2K-1}A(z^{-2})\} \end{cases}, \quad (2)$$

where K is integer, and $A(z)$ is an allpass filter of order N and defined by

$$A(z) = z^{-N}\frac{\sum_{n=0}^{N} a_n z^n}{\sum_{n=0}^{N} a_n z^{-n}}, \quad (3)$$

where a_n is real and $a_0 = 1$. It can be easily verified that $H(z)$ and $G(z)$ in Eq.(2) satisfy the orthonormality condition of Eq.(1). Assume that $\theta(\omega)$ is the phase response of $A(z)$, that is,

$$\theta(\omega) = -N\omega + 2\tan^{-1}\frac{\sum_{n=0}^{N} a_n \sin n\omega}{\sum_{n=0}^{N} a_n \cos n\omega}, \quad (4)$$

then the frequency responses of $H(z)$ and $G(z)$ are

$$\begin{cases} H(e^{j\omega}) = e^{-j(K+\frac{1}{2})\omega}\cos\{\theta(2\omega) + (K+\frac{1}{2})\omega\} \\ G(e^{j\omega}) = je^{-j(K+\frac{1}{2})\omega}\sin\{\theta(2\omega) + (K+\frac{1}{2})\omega\} \end{cases}, \quad (5)$$

which have an exactly linear phase and satisfy the following power-complementary relation;

$$|H(e^{j\omega})|^2 + |G(e^{j\omega})|^2 = 1. \quad (6)$$

Therefore, the design problem becomes the phase design of allpass filter $A(z)$. From the regularity requirement for wavelet bases, the wavelet filters $H(z)$ and $G(z)$ are required to have the maximally flat response. For the maximally flat wavelet filters, a closed-form solution has been given in [11] and [12] by

$$a_n = (-1)^n \binom{N}{n} \prod_{i=1}^{n} \frac{i - 1 - N + \frac{K}{2} + \frac{1}{4}}{i + \frac{K}{2} + \frac{1}{4}}. \quad (7)$$

A design method for the wavelet filters with the given degrees of flatness has been proposed in [12] also. It has been pointed out in [12] that an undesired zero and bump arise nearby $\omega = \pi/2$, as shown in Fig.1, when even N and $K = 4k+1$ or $4k+2$ or when odd N and $K = 4k$ or $4k+3$, where $k = 0, 1, \cdots, \lfloor \frac{N}{2} \rfloor$. See [12] in detail. To avoid this problem, we should choose $K = 4k$ or $4k+3$ when N is even, and $K = 4k+1$ or $4k+2$ when N is odd.

3. IMPLEMENTATION OF ALLPASS-BASED WAVELET FILTERS

In this section, we present an effective implementation of the allpass-based wavelet filters proposed in Section 2. We will describe the decomposition process only, and the reconstruction is done in the reversed order. First, we assume that $x(n)$ is input signal of length M, whose z transform is $X(z)$, and $\tilde{x}(n)$ is a periodic signal obtained by employing symmetric extension at the boundaries of $x(n)$. In the following, superscript tilde denotes a periodic signal, and capital letter is its z transform. It is known that $H(z)$ and $G(z)$ in Eq.(2) can be realized by using the polyphase structure shown in Fig.2. Then $\tilde{x}(n)$ must be passed through two allpass filters $A(z)$ and $A(z^{-1})$ after decimation. Now, we will demonstrate the decomposition process with an example of $M = 8$ and $K = 0$. $\tilde{x}(n)$ is obtained by doubling the boundary points of $x(n)$ and its period is $2M$. $\tilde{x}(n)$ is firstly decimated to get $\tilde{u}_0(n)$ and $\tilde{u}_1(n)$. Then $\tilde{u}_0(n)$ and $\tilde{u}_1(n)$ are periodic with period M and satisfy the symmetric relation;

$$\tilde{u}_0(n) = \tilde{u}_1(M-1-n), \quad (8)$$

that is,

$$\tilde{U}_0(z) = z^{-M+1}\tilde{U}_1(z^{-1}). \quad (9)$$

Note that when $K \neq 0$, the symmetric relation still holds, although the symmetric point is different. $\tilde{u}_0(n)$ and $\tilde{u}_1(n)$ are then passed through $A(z)$ and $A(z^{-1})$ to get $\tilde{v}_0(n)$ and $\tilde{v}_1(n)$;

$$\begin{cases} \tilde{V}_0(z) = \tilde{U}_0(z)A(z) \\ \tilde{V}_1(z) = \tilde{U}_1(z)A(z^{-1}) \end{cases}. \quad (10)$$

It is clear from Eqs.(9) and (10) that $\tilde{v}_0(n)$ and $\tilde{v}_1(n)$ satisfy the symmetric relation also;

$$\tilde{V}_0(z) = z^{-M+1}\tilde{V}_1(z^{-1}), \quad (11)$$

that is,

$$\tilde{v}_0(n) = \tilde{v}_1(M-1-n). \quad (12)$$

Therefore, the subband signals $\tilde{y}_0(n)$ and $\tilde{y}_1(n)$ can be computed by

$$\begin{cases} \tilde{y}_0(n) = \tilde{v}_0(n) + \tilde{v}_1(n) = \tilde{v}_0(n) + \tilde{v}_0(M-1-n) \\ \tilde{y}_1(n) = \tilde{v}_0(n) - \tilde{v}_1(n) = \tilde{v}_0(n) - \tilde{v}_0(M-1-n) \end{cases}. \quad (13)$$

It should be noted that only M samples of $\tilde{v}_0(n)$ are needed to get $M/2$ samples of $\tilde{y}_0(n)$ and $\tilde{y}_1(n)$. Thus we just need to pass $\tilde{u}_0(n)$ through $A(z)$ to get $\tilde{v}_0(n)$. In general, $A(z)$ has real poles and complex conjugate poles, then can be divided into first- and second-order allpass filters with real coefficients. In this paper, we

will use the maximally flat filters to meet the regularity requirement. It is found that the maximally flat allpass filters have only real poles, and is composed of first-order real allpass filters;

$$A(z) = \prod_{i=1}^{N} A_i(z) = \prod_{i=1}^{N} \frac{z^{-1} - \alpha_i}{1 - \alpha_i z^{-1}}, \qquad (14)$$

where α_i is real. Since α_i may be $|\alpha_i| < 1$ or $|\alpha_i| > 1$, $A(z)$ is generally unstable and includes a stable part $A^s(z)$ and anti-stable part $A^u(z)$, whose poles lie inside and outside the unit circle, respectively. For anti-stable part $A^u(z)$, we have

$$A^u(z^{-1}) = \prod_{i=1}^{N_1} \frac{z - \alpha_i}{1 - \alpha_i z} = \prod_{i=1}^{N_1} \frac{z^{-1} - \frac{1}{\alpha_i}}{1 - \frac{1}{\alpha_i} z^{-1}}, \qquad (15)$$

which is stable. Then $A^u(z)$ can be realized by reversing the input signal, passing it through stable $A^u(z^{-1})$ and then re-reversing the output signal, as shown in Fig.4. Since $A(z)$ is composed of the cascade of first-order real allpass filters, we consider implementation of first-order real allpass filters. First-order real allpass filters have many types of structures. The direct-form structure is shown in Fig.5. Its input-output relation is given by

$$\begin{cases} \tilde{s}_0(n) = \tilde{p}(n) + \tilde{s}_1(n-1) \\ \tilde{s}_1(n) = \alpha_i \times \tilde{s}_0(n) \\ \tilde{q}(n) = \tilde{s}_0(n-1) - \tilde{s}_1(n) \end{cases}, \qquad (16)$$

where only one multiplier and two adders are needed. Since the input signal is periodic, we need an initial value $\tilde{s}_0(-1)$ for starting the processing. $\tilde{s}_0(-1)$ can be computed by

$$\begin{aligned} \tilde{s}_0(-1) &= \tilde{p}(-1) + \alpha_i \tilde{p}(-2) + \alpha_i^2 \tilde{p}(-3) + \cdots \\ &\quad \cdots + \alpha_i^{L-2} \tilde{p}(-L+1) + \alpha_i^{L-1} \tilde{p}(-L) \\ &= \tilde{p}(-1) + \alpha_i \{\tilde{p}(-2) + \alpha_i \{\tilde{p}(-3) + \cdots \\ &\quad \cdots + \alpha_i \{\tilde{p}(-L+1) + \alpha_i \tilde{p}(-L)\} \cdots\}\}, \end{aligned} \qquad (17)$$

and

$$\tilde{s}_1(-1) = \alpha_i \times \tilde{s}_0(-1), \qquad (18)$$

where L multiplications and $L-1$ additions are needed for the initial value. Then the number of multiplications and additions required in first-order allpass filter implemantation for per output sample are $1+L/M$ and $2+(L-1)/M$, respectively. Hence, the wavelet filters $H(z)$ and $G(z)$ have a computational complexity with

$$\begin{cases} N_M = N(1 + \frac{L}{M}) \\ N_A = N(2 + \frac{L-1}{M}) + 1 \end{cases}, \qquad (19)$$

where N_M and N_A are the number of multiplications and additions for per output sample, respectively. Although L must be $L \to \infty$ theoretically, $L = 20 \sim 40$ is sufficient in practice. The computational complexity of filter order $N = 2 \sim 4$ with $M = 512$ and $L = 20$ are given in Table 1. In Table 1, the computational complexity of the Daubechies's 9/7-tap wavelet is also given for comparison purpose. It is seen that the filters of $N = 2$ and $N = 3$ have a lower computational complexity than the Daubechies's 9/7-tap wavelet.

4. EXPERIMENTAL RESULTS

In this section, we investigate the performance of the allpass-based wavelet filters for image compression. For the purpose of fair and consistent comparisons, we have chosen one of the best wavelet-based image codecs called SPIHT proposed in[10]. To save coding/decoding time, we have used the binary-uncoded version of SPIHT without entropy coding. It had been pointed out in [10] that about $0.3 \sim 0.6$ dB in PSNR can be improved with entropy coding, but at the expense of a larger execution time. The test images are Lena, boat, goldhill, and Barbara of size 512×512. The decomposition level is six. The distortion is measured by the peak signal to noise ratio (PSNR) between the original and reconstructed images. The allpass-based wavelet filters used here are the maximally flat filters given in [11] and [12].

4.1. Influence of K

It had been pointed out in [12] that the frequency responses of the wavelet filters are strongly influenced by K, and unapt K will cause an undesired zero and bump nearby $\omega = \pi/2$. Here, we investigate the influence of K on the compression performance. The results of Barbara obtained with $N = 2$ and $N = 3$ are shown in Fig.6 and Fig.7, respectively. It is seen that when N is even, $K = 0$ and $K = 3$ have a better result than $K = 1$ and $K = 2$, while $K = 1$ and $K = 2$ are better when N is odd. It is thought to be due to the influence of the undesired zero and bump nearby $\omega = \pi/2$. Also, the compression performance becomes worse with an increasing K. Therefore, we conclude that the optimal K is $K = 0$ or 3 when N is even, and $K = 1$ or 2 when N is odd. In the following, we choose $K = 0$ for even N and $K = 1$ for odd N.

4.2. Influence of N

To achieve a good compression performance, a reasonable regularity is required for wavelet filters. The regularity increases with an increasing N, but the computational complexity becomes larger. To have fast com-

putation, N should be small. We then investigate the influence of N on the compression performance. The results of Barbara and Lena are shown in Fig.8 and Fig.9, respectively. Note that $N = 0$ corresponds to the Haar wavelet. It is seen that the compression performance globally increases with an increasing N, but an asymptote is quickly attained. Above $N = 2 \sim 3$ for Lena and above $N = 3 \sim 4$ for Barbara, the performance does not improve much. Therefore, we conclude that $N = 2 \sim 3$ is sufficient for most natural images with predominantly smooth background such as Lena, boat and goldhill, and $N = 3 \sim 4$ for natural images with high-frequency components such as Barbara.

4.3. Comparison with Daubechies Wavelet

The compression performance comparisons with the Daubechies's 9/7-tap wavelet are shown in Table 2. It is seen that the filters of $N = 2 \sim 4$ have a better result than the Daubechies's 9/7-tap wavelet for Barbara, and are almost same for other images. To measure the subjective visual quality of the reconstructed images, the reconstructed images of Barbara with $N = 2$ and $N = 3$ are shown in Fig.11 and Fig.12. The original Barbara is shown in Fig.10, and the reconstructed image with the Daubechies's 9/7-tap wavelet is shown in Fig.13 also.

5. CONCLUSIONS

In this paper, we have presented an effective implementation of the allpass-based wavelet filters that simultaneously satisfy both the orthonormality and linear phase conditions for image compression. We have investigated the influence of the number K of delay elements on the compression performance, and found that the optimal K is $K = 0$ or 3 when N is even and $K = 1$ or 2 when N is odd. We have also found that the allpass filters of order $N = 2 \sim 4$ are sufficient for compression of natural images. Finally, we have shown through experimental results that the allpass-based wavelet filters proposed in this paper have a lower computational complexity than the conventional FIR wavelet filters, such as the Daubechies's 9/7-tap wavelet, with a comparable compression performance.

Table 1 Comparison of Computational Complexity with $M = 512$ and $L = 20$

Filter Type	No. of multiplier	No. of adder
Allpass-2	2.08	5.07
Allpass-3	3.12	7.11
Allpass-4	4.16	9.15
Daubeshies-9/7	4.50	7.00

6. REFERENCES

[1] I.Daubechies, "Ten Lectures on Wavelets", SIAM, Philadelphia, 1992.

[2] P.P.Vaidyanathan, "Multirate Systems and Filter Banks", Englewood Cliffs, NJ: Prentice Hall, 1993.

[3] M.Vetterli and J.Kovacevic, "Wavelets and Subband Coding", Prentice Hall PRT, Upper Saddle River, New Jersey, 1995.

[4] A.N.Akansu and M.J.T.Smith, "Subband and Wavelet Transforms: Design and Applications", Kluwer Academic Publishers, Boston, MA, 1996.

[5] M.J.T.Smith and S.L.Eddins, "Analysis/synthesis techniques for subband image coding", IEEE Trans. Acoust., Speech & Signal Processing, Vol.38, No.8, pp.1446–1456, Aug. 1990.

[6] M.Antonini, M.Barlaud, P.Mathieu and I.Daubechies, "Image coding using wavelet transform", IEEE Trans. Image Processing, Vol.1, No.2, pp.205–220, April 1992.

[7] M.Vetterli and C.Herley, "Wavelets and filter banks: theory and design", IEEE Trans. Signal Processing, Vol.40, No.9, pp.2207–2232, Sep. 1992.

[8] C.Herley and M.Vetterli, "Wavelets and recursive filter banks", IEEE Trans. Signal Processing, Vol.41, No.8, pp.2536–2556, Aug. 1993.

[9] J.M.Shapiro, "Embedded image coding using zerotree of wavelets coefficients", IEEE Trans. Signal Processing, Vol.41, No.12, pp.3445–3462, Dec. 1993.

[10] A.Said and W.A.Pearlman, "A new, fast, and efficient image codec based on set partitioning in hierarchical trees", IEEE Trans. Circuits & Systems for Video Technology, Vol.6, No.3, pp.243–249, June 1996.

[11] I.W.Selesnick, "Formulas for orthogonal IIR wavelet filters", IEEE Trans. Signal Processing, Vol.46, No.4, pp.1138–1141, April 1998.

[12] X.Zhang, T.Muguruma and T.Yoshikawa, "Design of orthonormal symmetric wavelet filters using real allpass filters", Signal Processing, accepted for publication.

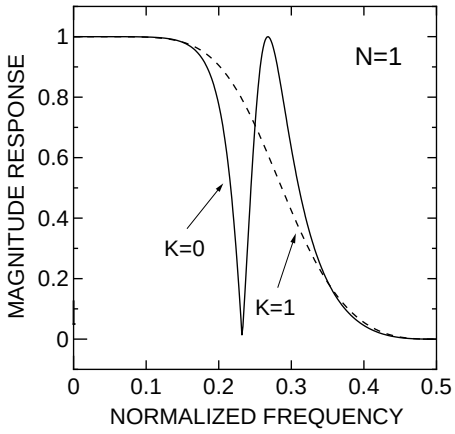

Fig.1 Magnitude response of $H(z)$.

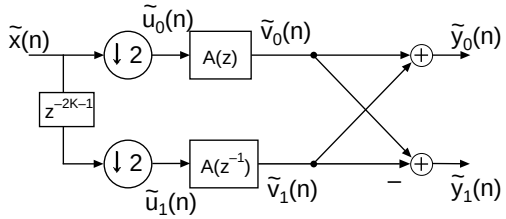

Fig.2 Polyphase structure.

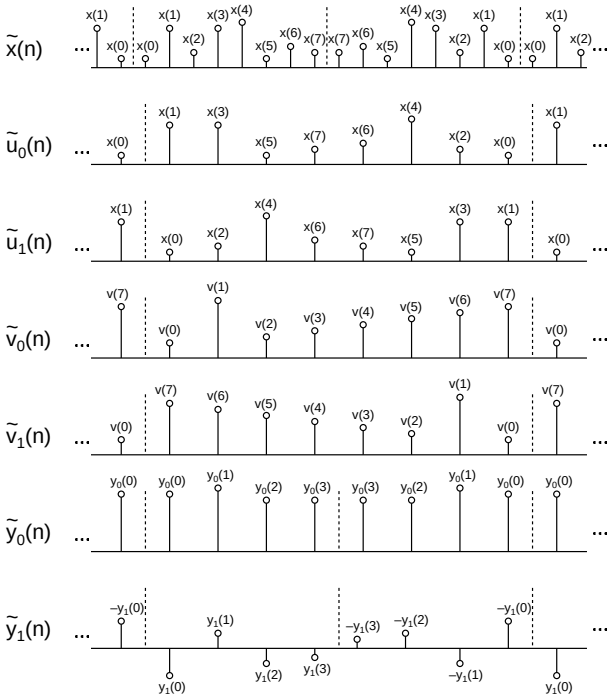

Fig.3 Decompositon process.

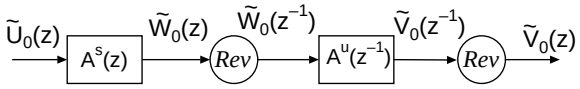

Fig.4 Realization of unstable allpass filters.

Table 2 Comparison of Coding Performance in dB

Image	bpp	N=2	N=3	N=4	D-9/7
Lena	1.0	**39.99**	**39.99**	39.97	39.81
	0.5	36.83	**36.84**	36.80	36.64
	0.1	29.71	29.70	29.63	**29.75**
boat	1.0	**38.36**	38.32	38.25	38.03
	0.5	**33.81**	33.78	33.74	33.68
	0.1	**26.85**	26.83	26.78	26.76
goldhill	1.0	35.90	**35.91**	35.89	35.80
	0.5	**32.55**	32.54	32.52	32.54
	0.1	**27.62**	27.59	27.59	27.60
Barbara	1.0	37.46	37.64	**37.71**	36.73
	0.5	32.24	32.45	**32.51**	31.59
	0.1	**24.39**	24.38	24.37	24.29

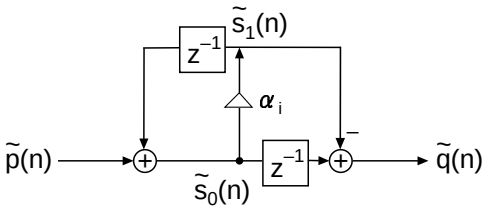

Fig.5 First-order allpass filter implementation.

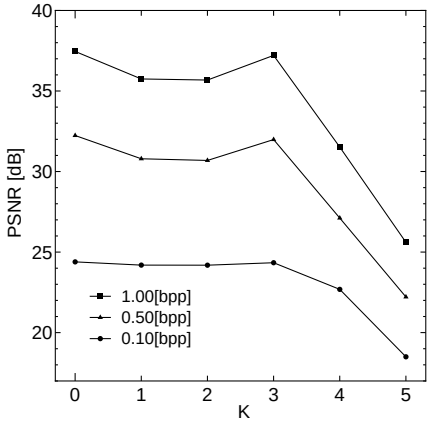

Fig.6 Peak SNR versus K ($N = 2$, Barbara).

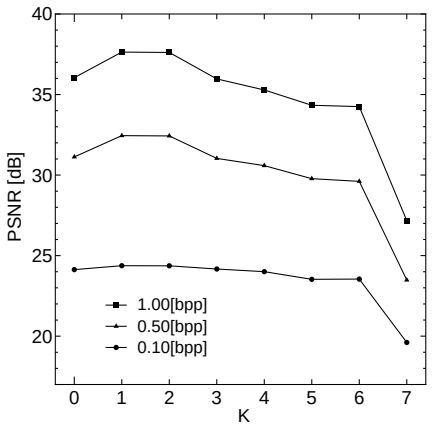

Fig.7 Peak SNR versus K ($N = 3$, Barbara).

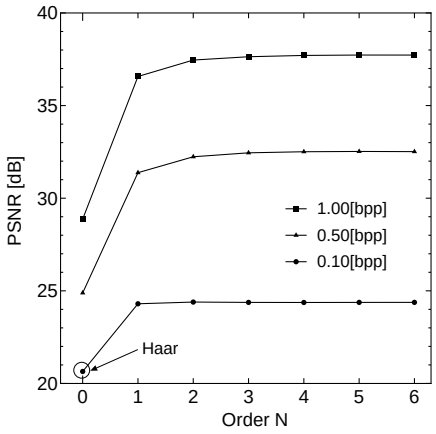

Fig.8 Peak SNR versus N (Barbara).

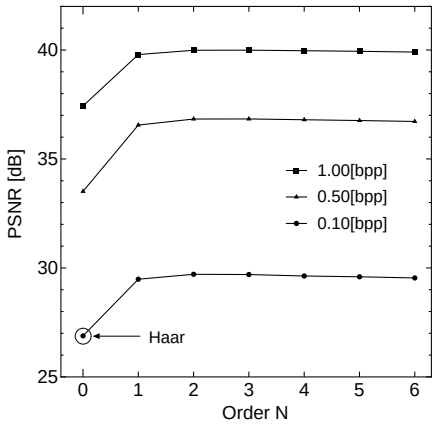

Fig.9 Peak SNR versus N (Lena).

Fig.10 Original Barbara (512×512, 8bpp).

Fig.12 Reconstructed image with $N = 3$ at 0.50bpp (PSNR=32.45dB).

Fig.11 Reconstructed image with $N = 2$ at 0.50bpp (PSNR=32.24dB).

Fig.13 Reconstructed image with Daubechies–9/7 at 0.50bpp (PSNR=31.59dB).